Design and Preliminary Tests of a Prototype CZT Imaging Array

T. Narita[1], J.E. Grindlay[1], J.A. Jenkins[1], M. Perrin[2], D. Marrone[1], R. Murray[1], B. Connell[1]

[1]Harvard-Smithsonian Center for Astrophysics, 60 Garden St., Cambridge, MA 02138

[2]Department of Astronomy, University of California at Berkeley

ABSTRACT

We report on the design and construction of a tiled Cadmium Zinc Telluride (CZT) detector array, suitable for use as an astronomical coded aperture imager. Four detector modules, each with $4 \times 4 \times 0.5$ cm of CZT, readout by two 128 channel XA type ASICs, have been built and incorporated into a detector focal plane array. A passive shield/collimator surrounded by plastic scintillator encloses the detector on five sides and provides a 40 degree field of view. In this paper, we present our performance goals and some preliminary calibration results.

Keywords: CdZnTe, pixellated imaging detectors, hard X-ray imaging

1. INTRODUCTION

There is considerable interest in the astronomical community, as summarized in the recent NRC Decadal Survey Report, for a mission to conduct a very high sensitivity all sky imaging hard x-ray survey. It has been more than 20 years since the only previous all sky survey was done by HEAO A-4.[1] Since then, considerable progress has been made in the study of galactic and extragalactic x-ray sources at the 0.1-10 keV energies. However, hard x-ray emission from black hole binaries (x-ray novae) and AGNs have shown that most of their radiated power comes out at 100 keV, and thus they are best identified and studied in the hard x-ray band. The EXIST mission[2] would provide a factor of nearly 1000 increased sensitivity over HEAO-A4, and should prove invaluable in the search and study of the most energetic processes in the universe.

To demonstrate some of the technology needed in constructing a full scale survey instrument, we have built a scientifically useful prototype for a balloon-borne payload. The CZT imaging detector was assembled with a prototype detector mounting and readout board developed for the IMARAD Gamma-Camera, with modifications for space flight data logging and background shielding. Due to the advances made in the ASIC readout and detector growth process in the past few years, the fabrication cost was kept to a minimum. Although some compromises were made in the detector readout, the complete system met our fundamental requirements of reasonable sensitivity up to 500 keV and the modularity required in scaling up to a 8 m^2 array.

One of the hurdles faced by astronomers and medical imaging scientist alike has been the low yield of high quality CZT with dimensions larger than 1 cm^2. The cost of building a large detector array on the order of 8 m^2 would be prohibitive if one were forced to pixellate and tile crystals 1 cm^2 at a time. Recently, IMARAD Imaging Systems, using the modified Horizontal Bridgman (HB) growth process, have successfully produced crystals up to 40 mm square without defects and at reasonable yield.[3] However, the drawback of the HB growth process is that the crystals typically have lower resistivity than that made from an alternate growth processes such as the High Pressure Bridgman. The lower resistivity leads to higher leakage current which significantly degrades the energy resolution below 60 keV. As a part of our detector program, we have found that the effective resistivity of a detector could be improved by creating a Schottky type contact on HB CZT. We have incorporated several types of Schottky contact detectors into our array to examine their uniformity and to compare against the ohmic type contacts used in standard IMARAD systems.

In this paper, we describe the design of the experiment and the fabrication process for the pixellated CZT detectors. We discuss the initial calibration performance of the detector array, and conclude with a remark on our future plans.

Further author information: (Send correspondence to T. Narita)
tnarita@holycross.edu

2. EXPERIMENT OVERVIEW

2.1. System

This is our third generation CZT experiment constructed for use in a high altitude balloon payload. The detector imaging array consists of four modules, arranged in a two by two array, which plugs into a printed circuit motherboard. Each of the modules contains four pixellated $20 \times 20 \times 5$ mm CZT crystals, and are readout by two 128 channel XAIM3.2 ASICs manufactured by IDE AS. The crystals are tiled in a two by two array, with the pixellated anodes epoxy bonded to the ASIC coupling board. The XA ASICs are mounted on the flip-side of the coupling board such that the entire electronic readout chain fits within the footprint of the CZT crystals. The total detector area is 64 cm^2.

In order to study the likely x-ray background in an astronomical survey imager, the detector array is fitted with a 40 degree field of view collimator/passive shield. The graded passive shield is composed of 1 mm thick tin and copper, surrounded by a 2mm thick lead. A large graded passive rear shield is mounted directly underneath the detector array and subtends $\sim 2\pi$ steradian solid angle. The combined collimator and rear shield blocks all line of sight to the detector from the side or the rear. To reject coincident events from charged particle cosmic rays, the collimator and rear shields are surrounded by 1 cm thick plastic scintillator and readout by six small photomultiplier tubes.

All the XA ASICs on the detector array are daisy-chained to a single XA controller box which supplies various bias voltages to the ASICs and handles the data readout. A flat ribbon cable, connecting the controller box to the detector motherboard, is used to pass control and data signals, and to provide power to the ASICs. The XA type ASIC has one drawback that only the pulseheight from the peak channel is digitized. It is often the case, especially at higher energies, that an incoming photon will deposit charge in several neighboring pixels through charge diffusion or Compton scattering. The ideal detector readout design would record the peak channel and a combination of several neighbor channels.

We did make one modification to the XA controller to output a fast shaped TTL compatible trigger pulse. This signal is used in coincidence with the output from the plastic scintillator shield PMTs to reject cosmic ray events. In the event of a trigger, the channel number and the digitized pulseheight are sent via a shielded cable to a PCI based National Instrument DAQ card running on a Pentium based single board computer. Trigger rates of up to 100k events/second are possible with this system. Current flight software allows runtime changes to the trigger threshold, and masking of noisy channels. Additional features, such as running a pulser to continuously calibrate the gain and offset during flight, can be easily implemented with the current hardware.

Since the ASICs are extremely sensitive to ground loops and pickup noise, the anticoincidence logic ground and the ASIC ground are kept isolated as much as possible. The analog and digital power to the XA controller box and the ASICs are supplied by an isolated supply for ground calibration, or by batteries during flight. The detector high voltage also must be powered by an isolated power supply to minimize the system noise.

2.2. Detectors

We fabricated sixteen pixellated detectors with a combination of metal contacts for our tiled imager array. In terms of pixel size and pitch, each of the $20 \times 20 \times 5$ mm crystals are identical; the pixel size is 1.9×1.9 mm and the pixel pitch is 2.5 mm. However for the contacts, we used a combination of gold, indium, and platinum for the various anodes and the cathodes. The interest in the variety of metal contacts is due to our recent results which showed that sputtered gold cathode acts as a blocking contact on IMARAD's HB growth CZT.[4] In Figure 4 we show the I-V curve measured from three different detectors with gold and indium electrode contacts. In particular, the IMARAD detector with gold contacts showed a rectified IV curve such that its effective resistivity at -700 V bias was an order of magnitude larger than the detector made with indium contacts. The effect of reduced leakage current improves the energy resolution, especially at energies below 60 keV (see Figure 6, Narita et al. (1999)[5]).

We had IMARAD make three detectors using e-beam evaporated gold cathode and indium anodes, and seven detectors were made at RMD Inc. in Watertown, MA using thermally evaporated gold on both electrodes. For comparison, we also purchased five standard indium anode and cathode contacted detectors from IMARAD. We experienced some difficulty in consistently fabricating good performance detectors with gold contacts. The CZT wafers were initially tested at IMARAD for uniformity and performance using indium contacts. However, once the indium contacts were polished off and replaced with gold contacts, we found that many of the detectors produced

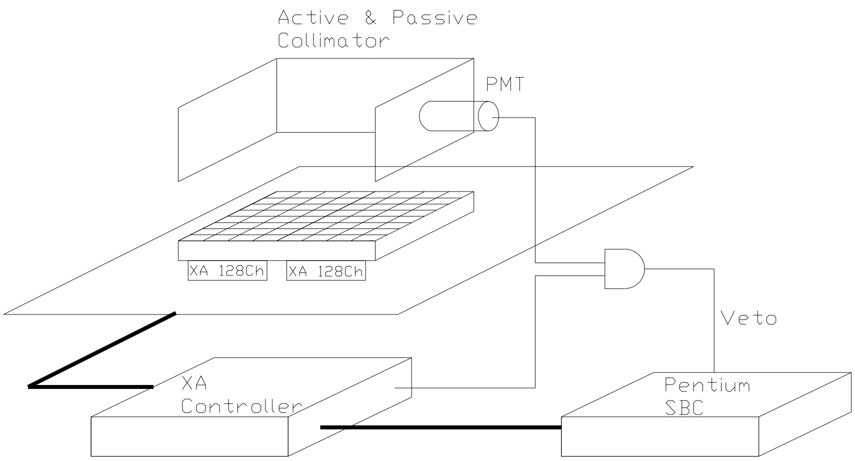

Figure 1. A schematic overview of the detector system. For clarity, only 1 (of 4) detector module is represented.

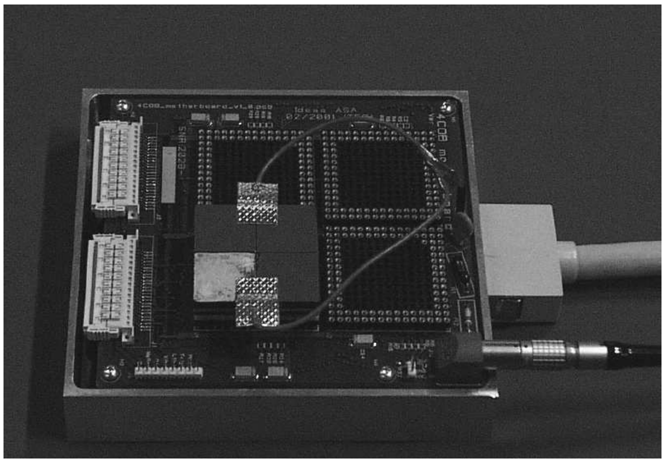

Figure 2. A close up photo of the entire detector array. Only one 4 cm $\times$ 4 cm detector module is shown. The modules contains 4 close-tiled 2cm $\times$ 2cm CZT crystals: 3 with Au cathode, In anode contacts, and 1 with In anode-cathode contacts. The cathode side (radiation side) of the single detector module is visible with a temporary HV bias connection attached.

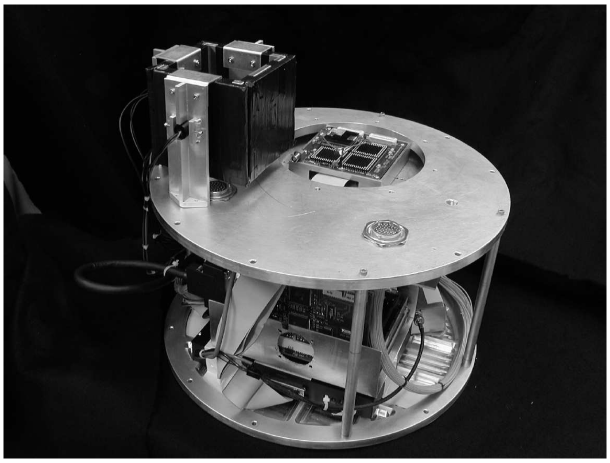

Figure 3. The flight system mounted in the pressure vessel with the sidewalls removed for clarity. The collimator has been moved off to the side to show the detector array.

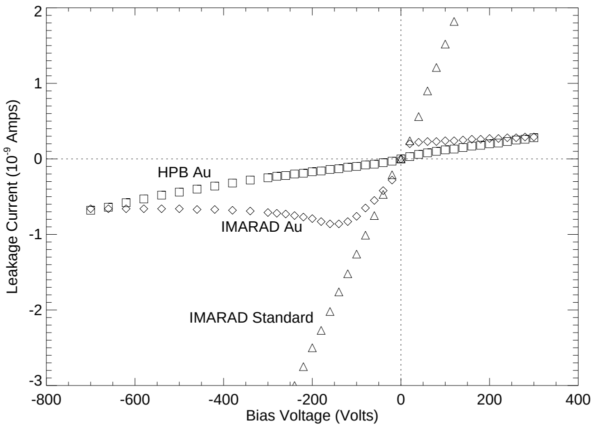

Figure 4. IV measurements for gold contacted CZT made by eV Products (HPB), IMARAD (IMARAD-Au), and indium contacted IMARAD CZT (IMARAD Standard). The gold on IMARAD CZT creates a Schottky contact resulting in a diode like behavior in the leakage current. The effective resistivity at -700V is approximately 10^{11} Ω-cm.

poor photopeaks. The yield of good detectors made with either IMARAD's or RMD's gold evaporation process was $\sim$ 50%. We speculate that the low yield in either gold deposition processes were due to non-optimal etching of the CZT and/or the lack of fine temperature and pressure control during the evaporation. As a possible future replacement for gold contacted detectors, we also made one detector at Goddard Space Flight Center using evaporated platinum anodes and cathode. The results from our platinum contacted CZT detectors will be reported separately.

3. DETECTOR PERFORMANCE

Although we fabricated four 4cm $\times$ 4cm detector modules, we decided to extensively test only one module while we analyzed the overall system performance. To incorporate all four modules, only minor software and hardware changes are needed. The single tested module (seen in Fig. 2) has three detectors with indium anodes and gold cathode, and one detector with indium on both the anodes and the cathode. The ASICs used on this module are of XAIM3 type ASICs supplied by IDE. The other three modules use the newer XAIM3.2, and the control biases

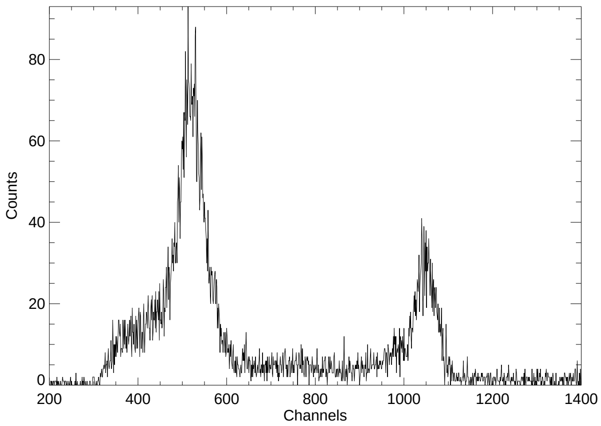

Figure 5. A sample low energy ^{133}Ba spectrum showing the detector threshold below $\sim$ 25 keV. The unresolved Barium 133 lines near 30 keV (left photopeak) and at 80 keV (right photopeak, which is also broadened by Pb fluorescence lines) are seen above the detector low energy cutoff.

in the XA controller are optimized for the XAIM3.2 ASICs. Although the two ASIC types are nearly identical, we expect even better overall performance with the XAIM3.2 modules.[6]

3.1. Detector Threshold

The sensitivity of a balloon-borne experiment is limited by the atmospheric cutoff of x-rays $< 25 - 30$ keV. However, for an eventual hard x-ray detector in space, the required low energy sensitivity would be $\sim$ 10 keV or lower. Such a low energy sensitivity is not usually a concern for a medical imaging camera since the x-rays used in those detectors are typically $\sim$ 140 keV. For our system, we tried to find the lowest usable energy threshold such that the low energy noise would not dominate our trigger.

We show in Figure 5 a low energy ^{133}Ba spectrum from one channel of one Au-In detector showing the family of lines near 30 keV and 80 keV line. The entire 30 keV Gaussian line is present , and the instrument threshold is $\sim$ 20 keV. Although the channel to channel variation in gain affects the discriminator cutoff in energy, we found that on many of the channels, the operating threshold could be lowered to below 25 keV. We are working to further reduce the threshold with improved grounding and RF shielding around the ASICs.

3.2. Detector Gain

The gain variation from pixel to pixel was measured by comparing the photopeak positions of ^{241}Am 60 keV and ^{57}Co 122 keV lines. Figure 6 shows the image of the pixel gain and the histogram of the distribution. We found that the pixel to pixel gain varied from 0.085 to 0.1 kev/ADC channel, with an average value of $\sim$ 0.09 keV/channel. The distribution appears to be skewed towards the higher gain pixels, which can be seen in the detector image as the collection of lighter colored pixels in the upper left quadrant. However, most of the channels show a fairly tight range in gain which will allow us to use a single low energy threshold for all the pixels.

3.3. Energy Resolution

To determine the energy resolution, we uniformly illuminated the module with a ^{57}Co source and measured the photopeak FWHM for each pixel. We found that three Au-In combination of detectors had a typical 122 keV FWHM of $\sim$ 5%. However, the In-In contacted detector had a very poor energy resolution of 7% – 12%. The In-In detector, with its higher leakage current, ought to have worse energy resolution than the gold-indium detectors. However, the FWHM difference at 122 keV would only be $\sim$ 1% at our current system noise of $\sim$ 400 e$^-$. The poor performance could not be attributed to a bad ASIC since one of the ASICs reads out the channels from two of the Au-In detectors in addition to the In-In detector. Since we cannot retest the crystals once they are bonded to

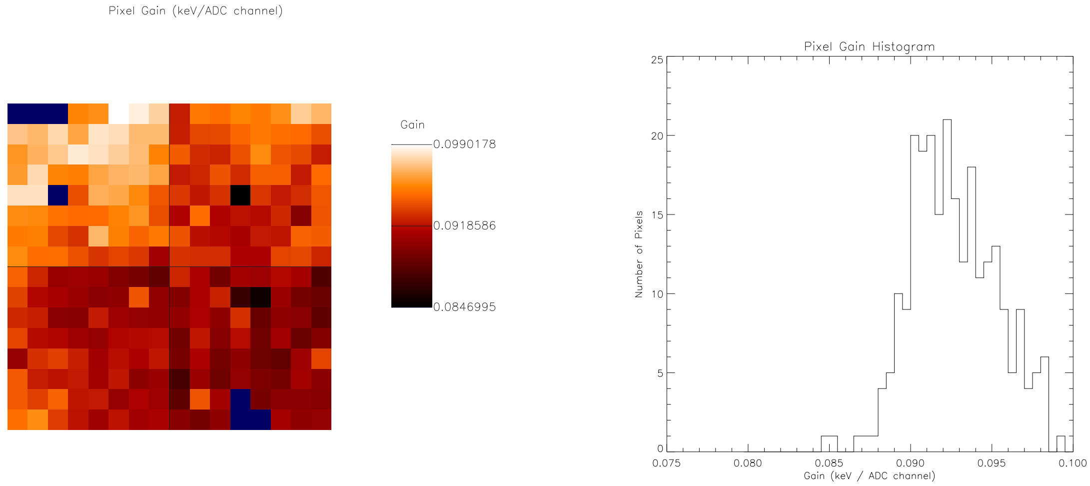

Figure 6. Detector image showing the gain map (left), and a histogram plot of the gain distribution (right). The gain distribution has a high gain tail, which is due to the cluster of high gain pixels seen in the upper left quadrant of the detector. The pixels on the three Au-In detectors where the gain could not be accurately measured are marked in black.

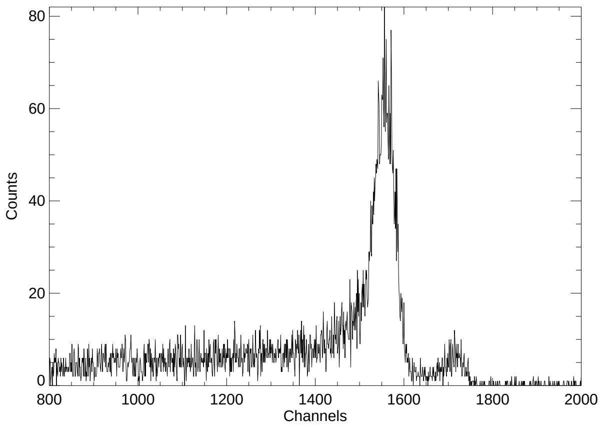

Figure 7. A sample ^{57}Co spectrum taken from one of the Au-In detectors. The 122 keV FWHM energy resolution is $\sim 5\%$.

the ASIC coupling board, we speculate that the poor performance was caused by either a problem in contacting or structural defects in the crystal which degraded the electron mobility.

In Figure 7 we show a sample ^{57}Co spectrum taken from one of the three good gold-indium detectors. We also show in Figure 8 an image of the energy resolution across the detector module and a histogram plot of the distribution. Among the pixels on the three good detectors, we found that the FWHM distribution could be well fit by a Gaussian, with mean 5% and (approximate) FWHM 2% (i.e. values of Gaussian distribution for pixel FWHM values). All the pixels with energy resolution greater than $7-8\%$ are from the In-In detector.

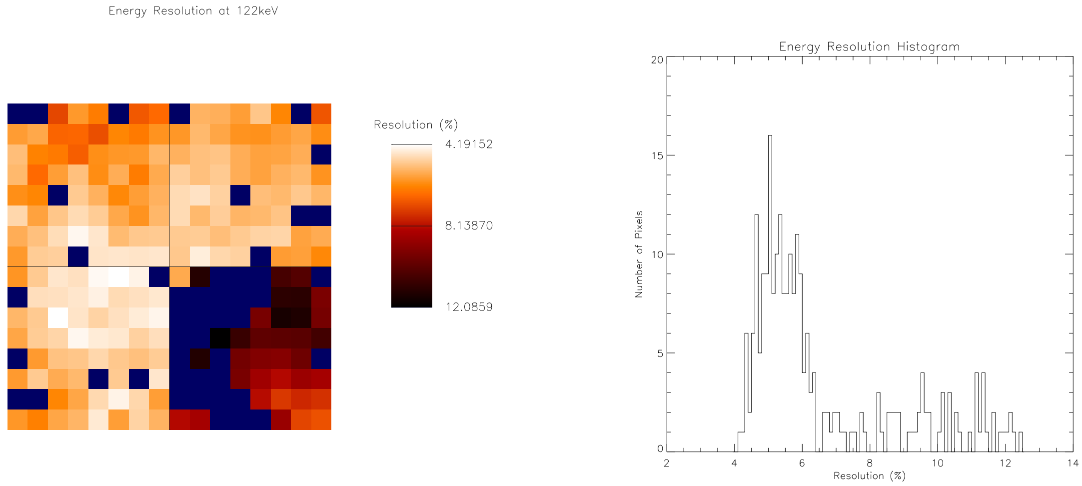

Figure 8. Detector image showing the FWHM energy resolution for each pixel (left), and a histogram plot of the energy distribution (right). The lower right quadrant of the image, with mostly dark colored pixels, corresponds to the indium-indium contacted detector. The Gaussian-like distribution of pixels are from the three Au-In detectors, while the scatter of large FWHM points are from the In-In crystal. Pixels on the three good detectors where the energy resolution could not be accurately determined are marked in black.

3.4. Detector Photopeak Efficiency

The detector photopeak efficiency compares the number of x-ray events where the charge is completely collected against events where the charge is only partially collected. In semiconductors like CZT where the charge carrier trapping is significant, relying on the small pixel effect[7] or tuning the detector bias[8] can minimize the number of incomplete charge collection events from appearing in the low energy tail. We fit each photopeak with a Gaussian and an exponential tail, and we define the photopeak efficiency as a ratio of the counts in the Gaussian component to the total number of events in the range of -5σ to $+2.5\sigma$ around the Gaussian center.

For a HB CZT detector with 1.9 mm square pixels on a 5 mm thick substrate, the typical photopeak efficiency has been previously found to be $\sim 76\%$.[4] We show the results from our detector module in Figure 9. The photopeak efficiency measured from our detector module varied from $70\% - 85\%$, with the peak of the distribution occurring $\sim 77\%$. Within the bulk of the three good crystals (excluding the edge pixels), the charge transport property appears uniform.

4. CONCLUSIONS

In preparation for a future mission such as EXIST, we have built a prototype imaging CZT detector for hard x-ray astronomy. The balloon payload instrument is optimized as a large field of view detector in a part of a coded aperture telescope. The detector is surrounded on five sides by a passive/plastic shielding to lower and reject the background, and the detector array is positioned inside a 40 degree field of view collimator. Stemming from a maturing crystal growth process and integrated readout electronics technology, the detector was built largely of commercially available components borrowed from the medical imaging industry. As such, some compromises were made in the design which are not ideal for an astronomical instrument. However, our initial calibration shows that the overall detector response appears uniform. Also, the compact tiling design and ASIC readout below the array allows for planar tiling of multiple detector modules.

Our initial calibration and testing of the detector has found that majority of the pixels are working at their expected level of noise and photopeak response. We have verified that the detector system could operate down to ~ 25 keV low energy threshold, which is near the atmospheric cutoff at a balloon float altitude. Due to contact problems or

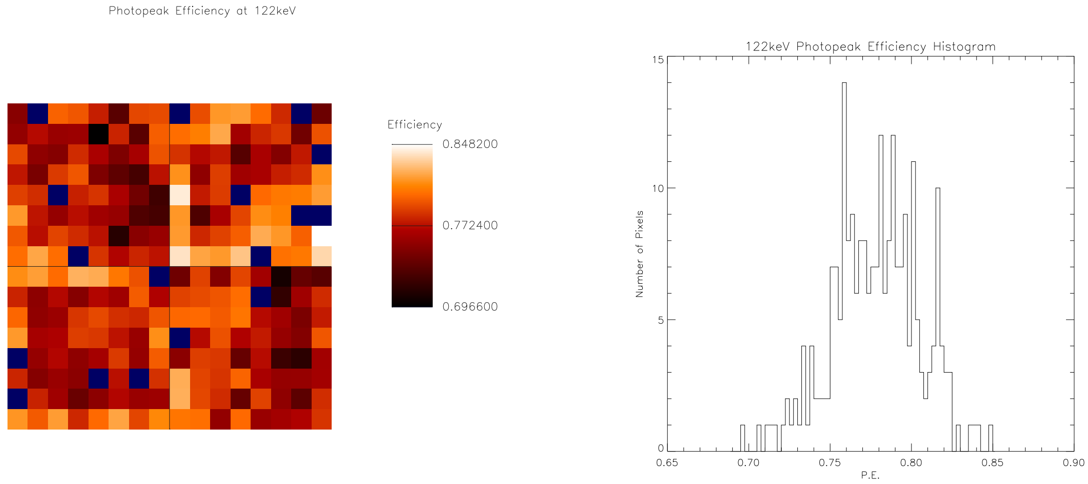

Figure 9. Detector image showing the 122 keV photopeak efficiency for each pixel (left), and a histogram plot of the distribution (right). The photopeak efficiency appears uniform over the bulk of the three good detectors (lower right quadrant is the bad detector) and the distribution is clustered $\sim 77\%$. Pixels on the three good detectors where the photopeak efficiency could not be accurately determined are marked in black.

crystal defects, one out of the four detectors performed poorly. However the remaining three CZT detectors showed good energy resolution and well distributed photopeak efficiency consistent with previous measurements.

Our future goals are to improve the threshold and noise performance with all four detector modules in place, and fly the experiment on a balloon with a 0.64 mm thick Tungsten coded mask. This will allow us to image the bright x-ray sources, Crab and CygX-1, at energies less than 100 keV, and at the same time conduct a CZT detector background (imaging) measurement at balloon altitudes for this prototype imager. The addition of a cathode readout is also planned, which will further reduce the detector background on upcoming balloon flights.

ACKNOWLEDGMENTS

We are grateful to Uri El-Hanany at IMARAD Imaging Systems, and Terje Orskaug and Einar Nygard at IDE AS, for their assistance in the design and fabrication of the XAIM3.2 ASIC system. We also thank Paul Bennett and Kanai Shah at RMD, and Carl Stahle and Brad Parker at GSFC, for their assistance in CZT detector fabrication. This work was supported in part by NASA grants NAG5-5103 and NAG5-5209.

REFERENCES

1. Levine, A.M. et al. *ApJS* **54**, p. 581, 1984.
2. J. Grindlay et al. *Proc. Gamma2001 Symposium* **AIP Conference Series**, in press.
3. T. Schlesinger, B. Brunett, H. Yao, J. VanScyoc, R. James, S. Egarievwe, K. Chattopadhyay, X. Ma, A. Burger, N. Giles, U. El-Hanany, A. Shahar, and A. Tsigelman, "Large volume imaging arrays for gamma-ray spectroscopy," *Presented at II-VI Workshop* , 1998.
4. T. Narita, P. Bloser, J. Grindlay, and J. Jenkins, "Development of gold contacted flip-chip detectors with IMARAD CZT," in *Hard X-Ray, Gamma-Ray, and Neutron Detector Physics III*, R.B.James and R. Schirato, eds., *Proc. SPIE* **4141**, p. 89, 2000.
5. T. Narita, P. Bloser, J. Grindlay, J. Jenkins, and H. Yao, "Development of IMARAD CZT detectors with pin contacts," in *Hard X-Ray, Gamma-Ray, and neutron detector physics*, R. James and R. Schirato, eds., *Proc. SPIE* **3768**, p. 55, 1999.
6. T. Orskaug *Private Communication* .

7. H. Barrett and J. Eskin, "Charge transport in arrays of semiconductor gamma-ray detectors," *Phys. Rev. Lett.* **75**, pp. 156–159, 1995.
8. T. Schlesinger, M. Greaves, S. Ross, B. Brunett, J. V. S. III, and R. James, "Role of uniformity and geometry in IMARAD-type gamma-ray spectrometers," *Proc. SPIE* **3768**, p. 16, 1999.